PCCP

PAPER

View Article Online
View Journal

Familie asymmetrically functionalized germanene films as promising quan spin Hall insulators

Citethis:DOI:10.1039/d0cp06231f

Received 2nd December 2020,
Accepted 22nd January 2021 DOI:
10.1039/d0cp06231f

rsc.li/pccp

Lawrence Shi[a] and Qiliang Li*[ab]

Topological insulators (TIs), exhibiting the quantum spin Hall (QSH) effect, are promising for developing dissipationless transport devices that can be realized under a wide range of temperatures. The search for new two-dimensional (2D) TIs is essential for TIs to be utilized at room-temperature, with applications in optoelectronics, spintronics, and magnetic sensors. In this work, we used first-principles calculations to investigate the geometric, electronic, and topological properties of GeX and GeMX (M = C, N, P, As; X = H, F, Cl, Br, I, O, S, Se, Te). In 26 of these materials, the QSH effect is demonstrated by a spin–orbit coupling (SOC) induced large band gap and a band inversion at the G point, similar to the case of an HgTe quantum well. In addition, engineering the intra-layer strain of certain GeMX species can transform them from a regular insulator into a 2D TI. This work demonstrates that asymmetrical chemical functionalization is a promising method to induce the QSH effect in 2D hexagonal materials, paving the way for practical application of TIs in electronics.

I. Introduction

Recently, topological insulators (TIs), materials with a bulk band gap and gapless surface states that are protected by time-reversal symmetry, have generated great interest in condensed matter physics and materials science.[1–6] Time-reversal symmetry causes the propagation direction of surface directions to be aligned with their spin, leading to dissipationless edge transport channels and the absence of backscattering, the unique hallmark of TIs.[7–10] Three-dimensional (3D) TIs have surface states consisting of an odd number of Dirac cones and are characterized by a Z_2 invariant of n = 1.[11–14] So far, many 3D TIs, including Bi_2Se_3, Bi_2Te_3, and Sb_2Te_3 have been verified experimentally.[1,6,15]

Recent progress on TIs has shifted towards discovering twodimensional (2D) TIs, also known as quantum spin Hall (QSH) insulators. Using the Bernevig–Hughes–Zhang (BHZ) model, the HgTe quantum well was confirmed to be the first 2D TI via a spin–orbit coupling (SOC) induced band inversion in the valence band.[16] However, the bulk gap is too small and the QSH is only observed at temperatures below 10 K, making them unrealistic for practical applications.[17] Other studies show CdTe, InAs, and GaSb quantum wells to be a similar case and exhibit similar properties.[16–18] Nevertheless, 2D TIs generally outperform their 3D TI counterparts due to their better flexibility and ability to be integrated into electronic devices.[19] Additionally, 2D TIs have robust edge states that prevent backscattering in all directions, which 3D TIs lack.[20] Following the initial success of these quantum wells, researchers began to search for new 2D TIs with large SOC band gaps.

Ever since its isolation in 2004, marking the beginning of a new era of 2D materials, graphene has been the subject of extensive research due to its superior mechanical and electronic properties with numerous applications.[21–24] Despite its tiny SOC band gap of only 10^3 meV, graphene showed remarkable initial promise and triggered researchers not only to continue studying graphene and its allotropes, but also to research other 2D hexagonal structures, such as silicene, germanene, stanene, plumbene, bismuthene, and antimonene. Although graphene and silicene have been fabricated experimentally, the practical 2D TI applications of these two materials are hindered by their tiny pristine band gaps of 10^3 meV[25] and 1.55 meV,[26] respectively. On the other hand, germanene has a significantly larger nontrivial gap,[27] making germanene more promising than either graphene or silicene in the field of 2D nanomaterials and 2D TIs. Germanene's isolation in 2014 for the first time gives much promise for practical applications.[28]

[a] Department of Electrical and Computer Engineering, George Mason University, Fairfax, Virginia 22030, USA. E-mail: qli6@gmu.edu

[b] Quantum Science and Engineering Center, George Mason University, Fairfax, Virginia 22030, USA

The success of germanene as a 2D TI promising for practical applications has stimulated the research of germanene-based systems. There are many methods to create new 2D TIs starting from a pristine material, including inducing a strain, placing the material on a substrate, and functionalizing the material.[29–33] However, by placing materials on substrates, the topological order may be destroyed via interactions between the material and substrate.[10] On the other hand, chemical functionalization and strain engineering are powerful tools for creating new 2D TIs with desirable properties. For example, it has been shown that the functionalization of 2D hexagonal structures can be tuned to exhibit the QSH effect under moderate tensile strains.[10,19,20,27,29,34–39] In these systems, the s orbitals with stronger SOC interactions, which dominate the states around the Fermi level, replace the original p orbitals with much weaker SOC interaction and thus enhance the gaps. Thus, we seek to research functionalized and strained germanene monolayers and evaluate their 2D TI potential.

The asymmetric functionalization of these germanene is another promising method to induce the QSH effect. For example, GeHN was discovered to be a large-gap TI under moderate strains.[40] Other than this work, 2D TIs created via the asymmetric functionalization of 2D hexagonal structures have not been studied in the literature. Similarly, asymmetrically functionalized stanene was shown to exhibit the quantum anomalous Hall effect, with both SnHN and SnOH being 2D TIs.[41] These studies indicate that asymmetric functionalization of 2D materials with honeycomb lattices is an effective way of producing new, large-gap TIs. However, there has been little research on asymmetrically functionalized systems compared to the vast documentation of symmetric systems in the literature. Thus, we believe that asymmetrically functionalized germanenes show promise in becoming excellent TIs, and we are motivated to conduct a large-scale study of such materials. In this paper, we document several novel families of 2D TIs in asymmetrically functionalized germanene films. We calculated the relaxed structures, bulk band structures, and partial density of states (PDOS) of GeX and GeMX (M = C, N, P, As; X = H, F, Cl, Br, I, O, S, Se, Te). The BHZ model indicates that many of these materials are 2D TIs with substantial band gaps that are likely to have practical room-temperature applications. In addition, the result indicated that the strain in functionalized germanenes has an important impact on TI transition.

II. Methods

The geometric, electronic, and topological properties of the materials studied were investigated using first-principles methods based on density-functional theory (DFT)[42,43] with a plane-wave basis set using the Ab initio code PWSCF package of Quantum Espresso.[44] Ultrasoft approximations and exchange correlation functionals in the generalized gradient approximation Perdew– Burke–Ernzerhof approximation (GGA-PBE) were used. Scalarrelativistic (full-relativistic) pseudopotentials were used for non-SOC (SOC) simulations. The Broyden–Fletcher–Goldfarb–Shanno (BFGS) method was employed for the structural optimization.

The self-consistent field (SCF) criterion for energy convergence was 10^6 Ry. For the bulk materials, the kinetic energy cutoff and vacuum distance were 50 Ry and 30 Å, respectively. For the structural optimization, the convergence threshold for the maximum absolute force on each atom was set to 10^3 Ry per bohr. The first Brillouin zone of the unit cell is sampled with a 2 2 1 Monkhorst–Pack grid for all systems.

III. Results and discussion

Fig. 1 illustrates the geometric structures of asymmetrically functionalized germanene. Pristine germanene has a very similar atomic structure to graphene and, like graphene, has both threefold rotational symmetry and inversion symmetry. Each Ge atom is covalently bonded to three other Ge atoms and either an M or X atom, leaving no lone pairs of electrons. Unlike graphene, pristine germanene prefers a low-buckled configuration with a buckling height of 0.58 Å to 0.78 Å.[45] Interestingly, GeX and GeMX films also prefer a low-buckled configuration with generally larger buckling heights of 9–51%, compared to that of pristine germanene. Their lattice constants and Ge–Ge bond lengths are quite different than those of pristine germanene, 4.03 Å and 2.44 Å, respectively. The preferred low-buckled configuration of pristine germanene, GeX, and GeMX indicates that both sp^2 and sp^3 bonding are present.[46] The Ge–M and Ge–X bonds occur on both sides of the low-buckled germanene plane in an alternating way. Thus, the crystal structures of GeX and GeMX films can be classified as a hexagonal Bravais lattice, similar to the crystal structures of materials like silicene and stanene.

For each material, we fully relaxed the atomic structure with variable lattice parameters and atom positions. The lattice constants, bond lengths, buckling heights, and band gaps of all materials studied after relaxation are listed in Table 1. The lattice constants of GeX and GeMX vary depending on the material, significantly different than that of pristine germanene (4.03 Å)[47] and GeI (4.08 Å).[27] In addition, the Ge–M and Ge–X bond lengths varied significantly. Generally, the lattice

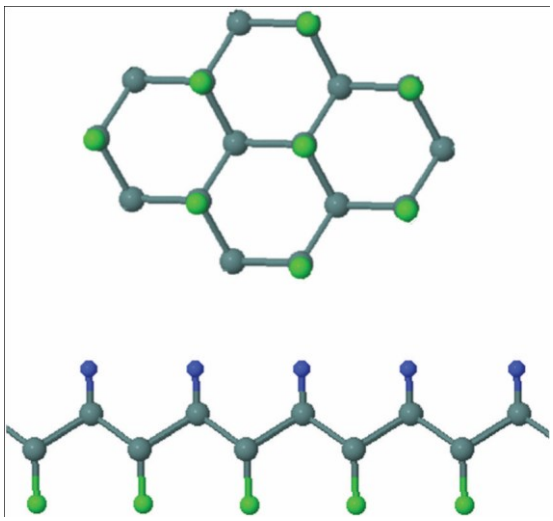

Fig. 1 The hexagonal lattice structure of GeMX from the top (top) and side (bottom) views. The teal atoms represent Ge, the green atoms represent M (N, P, As, C), and the blue atoms represent X (H, F, Cl, Br, I, O, S, Se, Te).

Table 1 Lattice constant (a), Ge–M bond length ($d_{Ge–M}$), Ge–X bond length ($d_{Ge–X}$), Ge–Ge bond length ($d_{Ge–Ge}$), buckling height (h), energy band gap without SOC (E_g), ba gap without SOC adjusted to HSE ($E_{g\text{-}HSE}$), band gap with SOC ($E_{g\text{-}SOC}$), and band gap with SOC adjusted to HSE ($E_{g\text{-}SOC\text{-}HSE}$) of GeMX (M = C, N, P, As; X = H, F, Cl, Br, I, O, S, S Te). HSE-gaps were calculated assuming a 30% underestimation of the PBE band gap. Indirect band gap is noted as ID. The four 2D TI materials marked in bold exhil significant SOC-based direct band gap at G point but close to zero indirect band gap with CBM at M point

System	a (Å)	$d_{Ge–M}$ (Å)	$d_{Ge–X}$ (Å)	$d_{Ge–Ge}$ (Å)	h (Å)	E_g (eV)	$E_{g\text{-}HSE}$ (eV)	$E_{g\text{-}SOC}$ (eV)	$E_{g\text{-}SOC\text{-}HSE}$ (eV)
Pristine Ge	4.030	—	—	2.440	0.630	0	0	0	0
GeH	4.030	—	1.560	2.387	0.758	1.112	1.589	0.963	1.376
GeF	4.114	—	1.794	2.409	0.662	0.541	0.773	0.492	0.703
GeCl	4.081	—	2.191	2.415	0.741	0.437	0.624	0.410	0.586
GeBr	4.075	—	2.381	2.408	0.821	0.261	0.373	0.131	0.187
GeI	4.080	—	2.557	2.417	0.762	0	0	0.308	0.440
GeO	4.116	—	1.710	2.390	1.247	0	0	0.061	0.087
GeS	3.860	—	2.110	2.241	1.154	0.040 (ID)	0.571	0.040 (ID)	0.571
GeSe	3.920	—	2.305	2.254	1.181	0	0	0.135	0.193
GeTe	4.140	—	2.542	2.403	0.920	0	0	0.026 (ID)	0.371
GeNH	3.890	1.788	1.591	2.369	1.055	0.779	1.113	0.640	0.914
GeNF	4.100	1.781	1.798	2.400	1.094	0.045	0.064	0.034	0.486
GeNCl	4.112	1.771	2.195	2.391	1.042	0.039	0.056	0.088	0.126
GeNBr	4.091	1.778	2.342	2.364	1.044	0.054	0.077	0.048	0.069
GeNI	4.120	1.771	2.564	2.379	1.053	0	0	0.119	0.170
GeNO	4.100	1.759	1.707	2.394	1.238	0.038	0.054	0.041	0.059
GeNS	3.975	1.766	2.081	2.328	1.294	0.008	0.011	0.058	0.083
GeNSe	3.919	1.769	2.250	2.288	1.262	0.054	0.077	0.048	0.069
GeNTe	4.016	1.768	2.564	2.296	1.180	0	0	0.196	0.280
GePH	3.810	2.238	1.570	2.373	1.021	0.444 (ID)	0.634	0.438 (ID)	0.626
GePF	3.717	2.210	1.790	2.308	1.034	0.097	0.139	0.088	0.126
GePCl	3.981	2.215	2.188	2.358	0.958	0	0	0.046	0.066
GePBr	4.190	2.209	2.325	2.459	0.859	0	0	0.082	0.117
GePI	4.037	2.212	2.558	2.355	0.947	0	0	0.073	0.104
GePO	3.830	2.191	1.712	2.473	1.228	0	0	0.077	0.110
GePS	3.883	2.248	2.107	2.343	1.256	0.056	0.080	0.056 (ID)	0.080
GePSe	3.702	2.211	2.263	2.469	1.052	0	0	0.116	0.166
GePTe	3.746	2.234	2.571	2.219	1.080	0	0	0 (ID)	0
GeAsH	4.005	2.378	1.581	2.488	0.919	0	0	0.093	0.133
GeAsF	3.964	2.347	1.795	2.482	0.849	0	0	0.196	0.280
GeAsCl	3.945	2.349	2.185	2.339	0.931	0	0	0.088	0.126
GeAsBr	3.971	2.345	2.331	2.366	0.916	0	0	0.113	0.161
GeAsI	3.990	2.351	2.561	2.407	0.930	0 (ID)	0	0 (ID)	0
GeAsO	3.880	2.347	1.713	2.363	1.179	0	0	0.145	0.207
GeAsS	3.639	2.366	2.110	2.400	1.103	0	0	0.138	0.197
GeAsSe	3.705	2.363	2.272	2.477	1.019	0	0	0.163	0.233
GeAsTe	3.771	2.370	2.574	2.452	0.952	0 (ID)	0	0 (ID)	0
GeCH	3.985	1.942	1.580	2.339	0.959	0.213	0.304	0.211	0.301
GeCF	3.826	1.915	1.798	2.415	0.935	0	0	0.073	0.104
GeCCl	4.182	1.909	2.203	2.549	0.900	0	0	0.056	0.080
GeCBr	4.151	1.899	2.316	2.711	0.762	0.114	0.163	0.135	0.193
GeCI	4.189	1.906	2.562	2.602	0.903	0	0	0.095	0.136
GeCO	4.030	1.906	1.714	2.412	1.192	0.064	0.091	0.096	0.137
GeCS	4.087	1.902	2.102	2.525	1.038	0	0	0.066	0.094
GeCSe	4.090	1.926	2.275	2.476	1.086	0	0	0.095	0.136
GeCTe	4.063	1.926	2.275	2.477	1.081	0	0	0.091	0.130

constants and Ge–X bond lengths trend upward as the X atom grows in size. Correspondingly, the lattice constants and Ge–M bond lengths trend upward as the M atom grows in size. The Ge–Ge bond length is an indicator of the intra-layer strain within the germanene layer. There is not a significant correlation between Ge–Ge bond lengths and buckling heights among GeX and GeMX systems. However, the Ge–

Ge bond length varies significantly with different combinations of M and X functionalization, indicating a remarkable effect of intra-layer strain. This indicates that regular insulators can be transformed into TIs by engineering the intra-layer strain in functionalized germanene films, which will be discussed in the last section. In addition, the 4 2D TI materials marked in bold in Table 1, GeTe, GePTe, GeAsI and GeAsTe, exhibiting band inversion with SOC at valence band maximum (VBM), thereby a direct band gap appearing at the G point, show zero indirect band gap due to the conduction band minimum (CBM) at M point. On the experimental side, TIs like the ones presented in this study have excellent optical properties, such as Kerr and Faraday rotation and near-infrared frequency transparency.[48,49] Thus, these materials may have interesting applications in optoelectronics and valleytronics.[50]

We plotted the energy band structures of all materials to analyze their electronic structures. It is well-known that PBE functional underestimates bandgaps by about 30% compared to those calculated using the Heyd–Scuseria–Ernzerhof (HSE) functional, the latter of which more accurately reflects the experimental band gaps.[51] Thus, we have also included the adjusted HSE band gaps in Table 1 for more accurate comparison with experimental results. Fig. 2–6 display the band structures of GeX, GeNX, GePX, GeAsX, and GeCX, respectively. Although there exists some variation in the band structures, most of them follow a very similar pattern. For all GeX and GeMX systems, the band gap (or lack thereof) occurs at the G point, whereas the valence and conduction bands intersect at the K point for pristine germanene.

Among all GeX and GeMX systems in this study, those observing the QSH effect, according to the BHZ model, are detailed in Table 2. For such systems, the energy band gap without SOC is unobservable, close to zero. However, the band gap opens up significantly when SOC is adopted in the simulation. The opening band gap arises from a downshifting of the VBM and an upshifting of the CBM when compared to their counterparts without SOC, a strong indicator of the QSH effect. Furthermore, a band inversion is exhibited at the G point, indicating the presence of a topological phase and evidence of topologically nontrivial systems. This band inversion is observed primarily at the VBM. The evolution from a single Dirac cone without SOC to a band inversion with SOC at the top of the valence band indicates that the bands representing the s and $p_{x,y}$ orbitals are also inverted.[10,30,52–55] The band structures are consistent with the BHZ model for TIs, where HgTe quantum wells were observed to have a similar characteristic.[16]

Within the GeX systems, the effect of SOC on the energy band structures and band gaps of the materials varied depending on the size of the X atom. For light X atoms, the weak SOC of the X atom has very little effect on the electronic properties of GeX. On the other hand, GeX systems with heavy X atoms like GeI and GeTe have strong SOC, causing the band gap to open up significantly and a band inversion to be induced. Interestingly, the band gap becomes indirect for GeS and GeTe systems

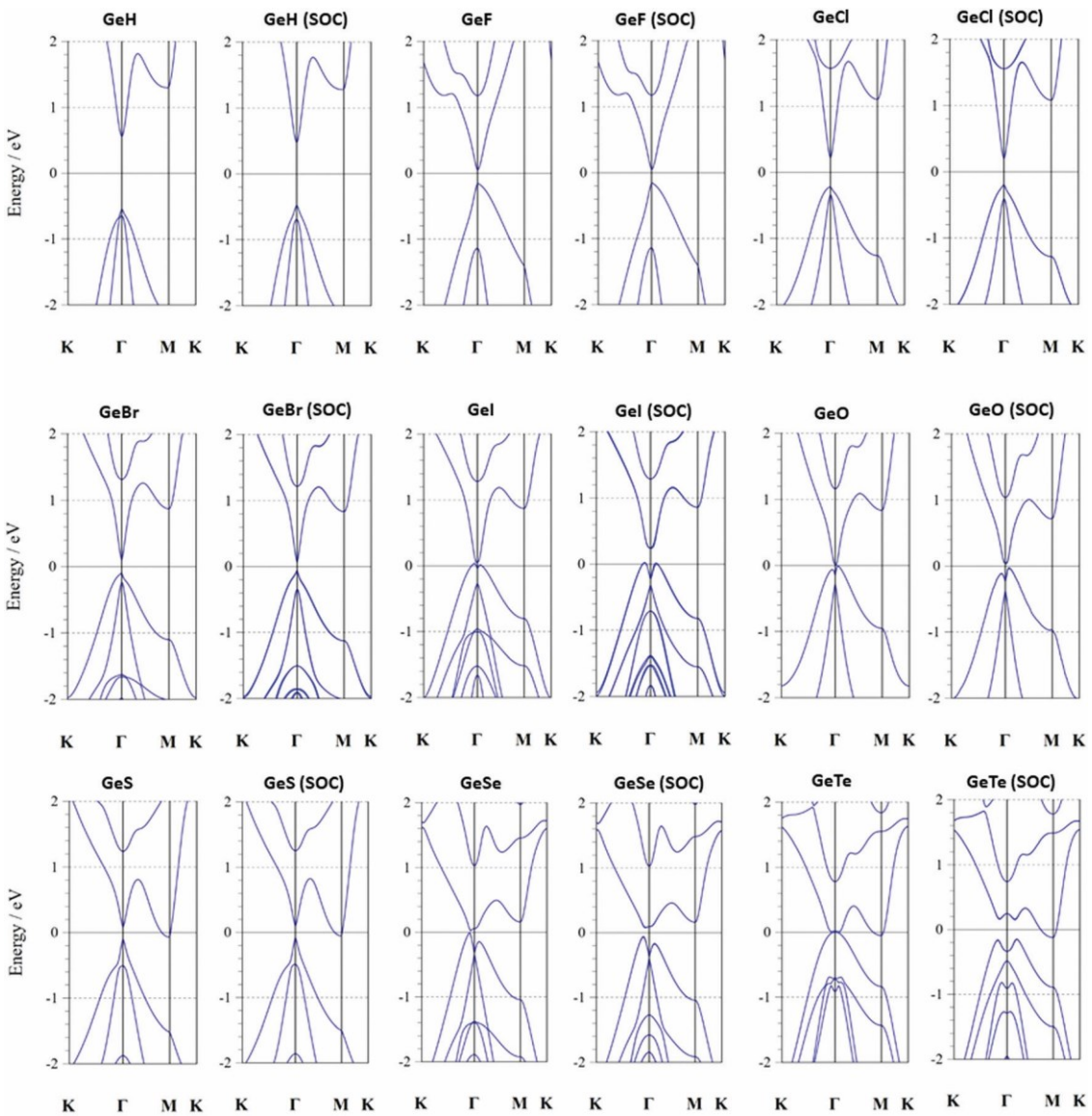

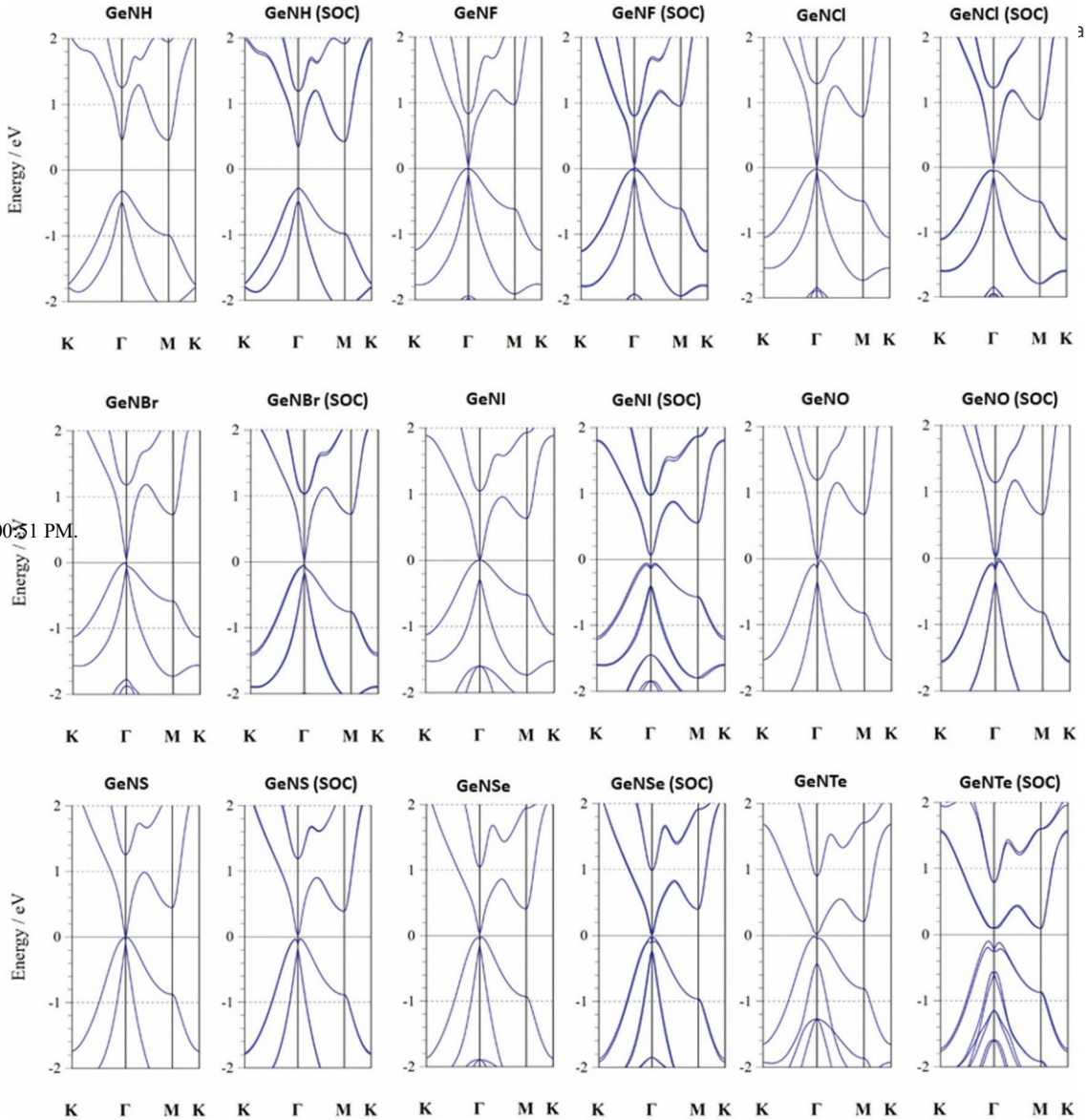

Fig. 2 Calculated band structures of GeX are shown, both with and without SOC as indicated. The Fermi level is set to 0 eV.

Fig. 3 Calculated band structures of GeNX are shown, both with and without SOC as indicated. The Fermi level is set to 0 eV.

due to the CBM at the M point dropping below the CBM at the G point.

For GeNX systems, a similar pattern is apparent, where SOC had little effect on the band structure of systems with light X atoms like GeNH, but a significant effect on that of systems with heavy X atoms like GeNTe. Due to the weak SOC of N atoms, the band gap was not significantly enlarged in most cases. The exceptions were GeNI and GeNTe, where SOC opened up the band gaps and induced a band inversion due to the strong SOC of the relatively heavy I and Te atoms. Nonetheless, most GeNX systems exhibited an SOC-induced band inversion, indicating that the main bottleneck to realizing the QSH effect in GeNX systems is the small band gap caused by the weak SOC of N atoms.

Compared to GeNX systems, more GePX systems exhibit the QSH effect due to the stronger SOC of P atoms. When SOC is induced, the band gaps at the G point increase considerably. We found that GePBr, GePI, GePO, and GePSe exhibit the QSH effect. Interestingly, GePH, GePS, and GePTe have indirect band gaps, although both the direct and indirect band gap of GePS is close to zero.

Many GeCX systems also observe similar transitions in the band structure when SOC is induced. GeCF, GeCCl, GeCI, GeCS, GeCSe, and GeCTe exhibited the QSH effect. These 2D TIs tend to have X atoms with strong SOC, as expected.

Compared to N, P, and C atoms, As atoms have considerably stronger SOC,[56] resulting in all GeAsX systems, including those with light X atoms like GeAsH, exhibiting an enlarged band gap and induced band inversion. All GeAsX systems exhibit the QSH effect and thus are 2D TIs, according to the BHZ model, although GeAsI and GeAsTe exhibit indirect band gaps with SOC whereas the CBM at the M point dips below the VBM at the G point.

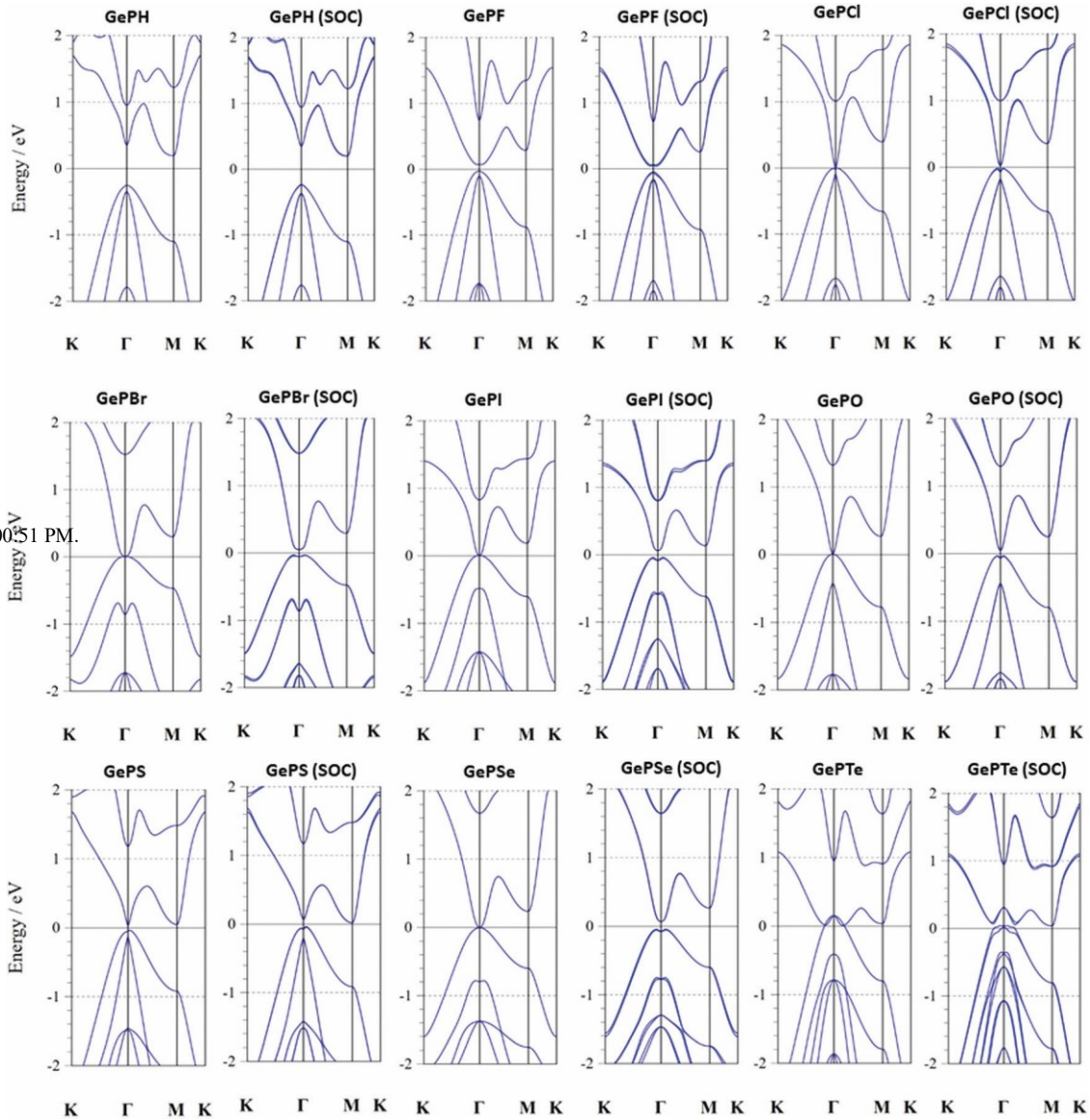

Fig. 4 Calculated band structures of GePX are shown, both with and without SOC as indicated. The Fermi level is set to 0 eV.

In addition, our study indicates that regular insulators can be transformed into 2D TIs by engineering the intra-layer strain in the functionalized germanenes. Fig. 7 shows the energy band structures of GeNBr under compressing and stretching strains, in corresponding to negative and positive changes in the Ge–Ge bond length, respectively. The 1% to +1% strain represents a change in the Ge–Ge bond length in comparison with that in the relaxed crystal structure. The GeNBr is clearly a regular insulator at compressing strain, zero strain and stretching strain less than 0.5%. The GeNBr is transformed into a TI when the strain is in a range of +0.5% to +2% whereas the VBM band inversion is observed with SOC. It returns to a regular insulator when the strain is larger than 2%, reaching a band gap of 0.4 eV at a strain of 3%. The result indicates that the intra-layer strain plays an important role in TI transition as it significantly affects the electronic energy band structure. Since such a small strain can be introduced by stretching the surfacefunctionalized germanenes or planting them onto a substrate with a larger crystal lattice, it is practical to obtain 2D TIs from regular 2D germanene insulators by strain engineering. Our study has further confirmed that even with an intra-layer strain from 2% to +2% in GeAsS, a 2D TI, the SOC-induced band gap and band inversion at the G point are well preserved, evidencing the robustness of the QSH state in GeMX systems. It should be noted that the GeAsS becomes a regular insulator with strain 4 +3%. These results indicate that strain engineering is a powerful tool for both transforming regular insulators into 2D TIs and preserving the QSH state in existing 2D TIs for similar systems.

In Fig. 8, we plotted the (PDOS) of GeAsS, a 2D TI, in order to further analyze the electronic structures of asymmetrically functionalized germanene and corroborate their band structures. The band structure and PDOS of GeAsS is representative of those of other valence regime and the $p_{x,y}$ orbitals of Ge within the conduction regime.

The band gaps of all 2D TIs presented in this study are significantly greater than 0.026 eV, the thermal energy at room temperature. Thus,

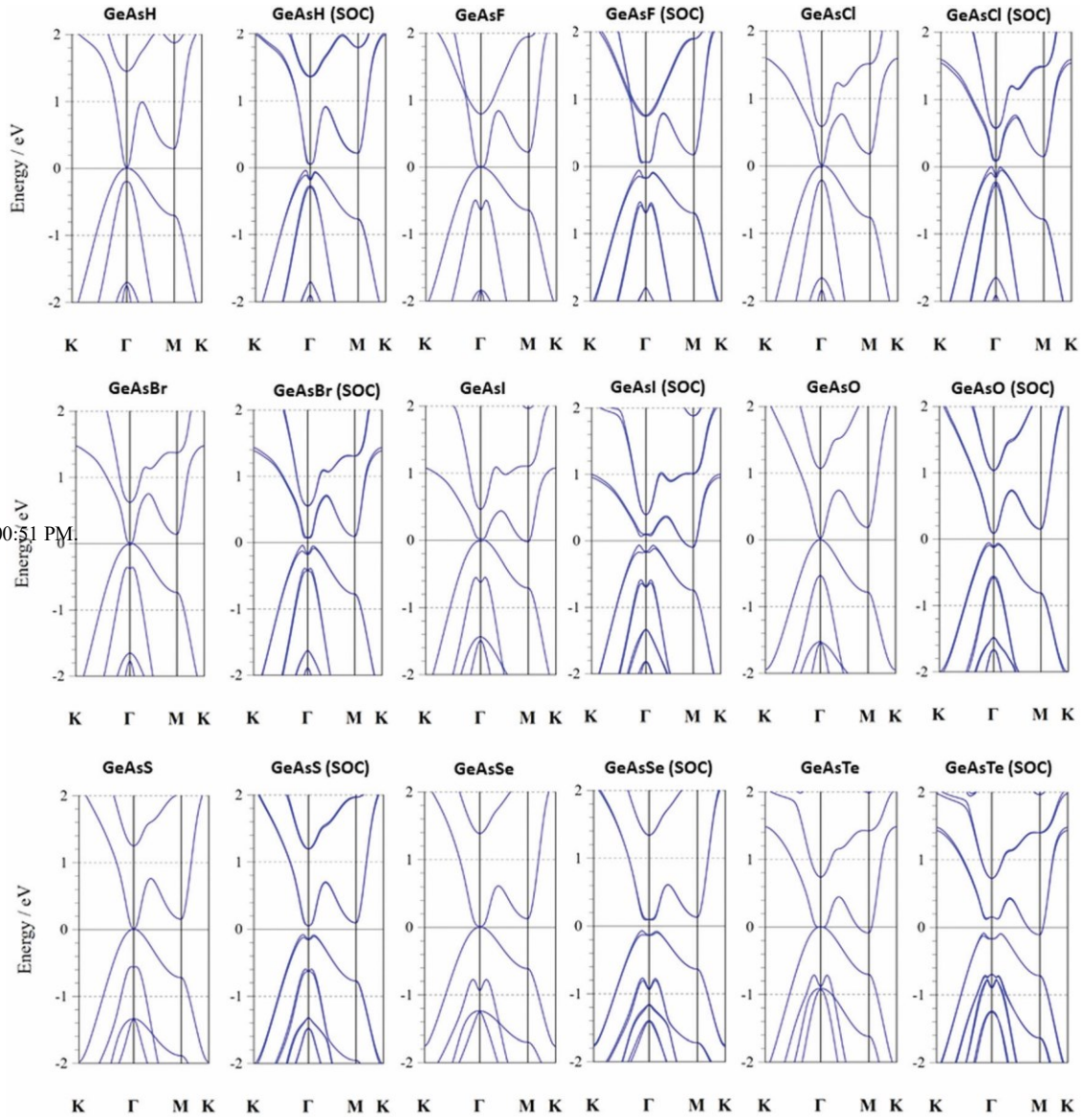

Fig. 5 Calculated band structures of GeAsX are shown, both with and without SOC as indicated. The Fermi level is set to 0 eV.

2D TIs reported in this study. All of the PDOS are consistent with the band structures; the band gap in the PDOS around 0 eV corresponds to the direct band gap in the band structure. The peaks of the s and p subshells of the Ge, As, and S atoms are almost perfectly aligned, with the major peaks at 1.83 eV, 1.09 eV, 0.52 eV, and 0.60 eV. The concurrent peaks among the different orbitals in the PDOS indicate that the Ge–Ge, Ge–As, and Ge–S bonds are all covalent and evidence the presence of hybridization between the s and p subshells in all atoms. The PDOS is dominated by the $p_{x,y}$ orbitals of As within the valence regime and the $p_{x,y}$ orbitals of Ge within the conduction regime.

These TIs are suitable candidates for the vast array of practical, room-temperature applications. The plethora of 2D TIs created via the asymmetric functionalization and strain engineering of germanene shows that these are effective methods of tuning the topological properties of and inducing the QSH effect in 2D hexagonal materials like germanene.

IV. Conclusion

We investigated the geometric, electronic, and topological properties of GeX and GeMX (M = N, P, As, C; X = H, F, Cl, Br, I, O, S, Se, Te) using first-principles calculations. In summary, we show that we are able to tune the topological properties of germanene-based systems through functionalization and asymmetrical functionalization. This study prompts the further investigation of asymmetric functionalized systems similar to germanene, like graphene, silicene, and stanene. Many GeX

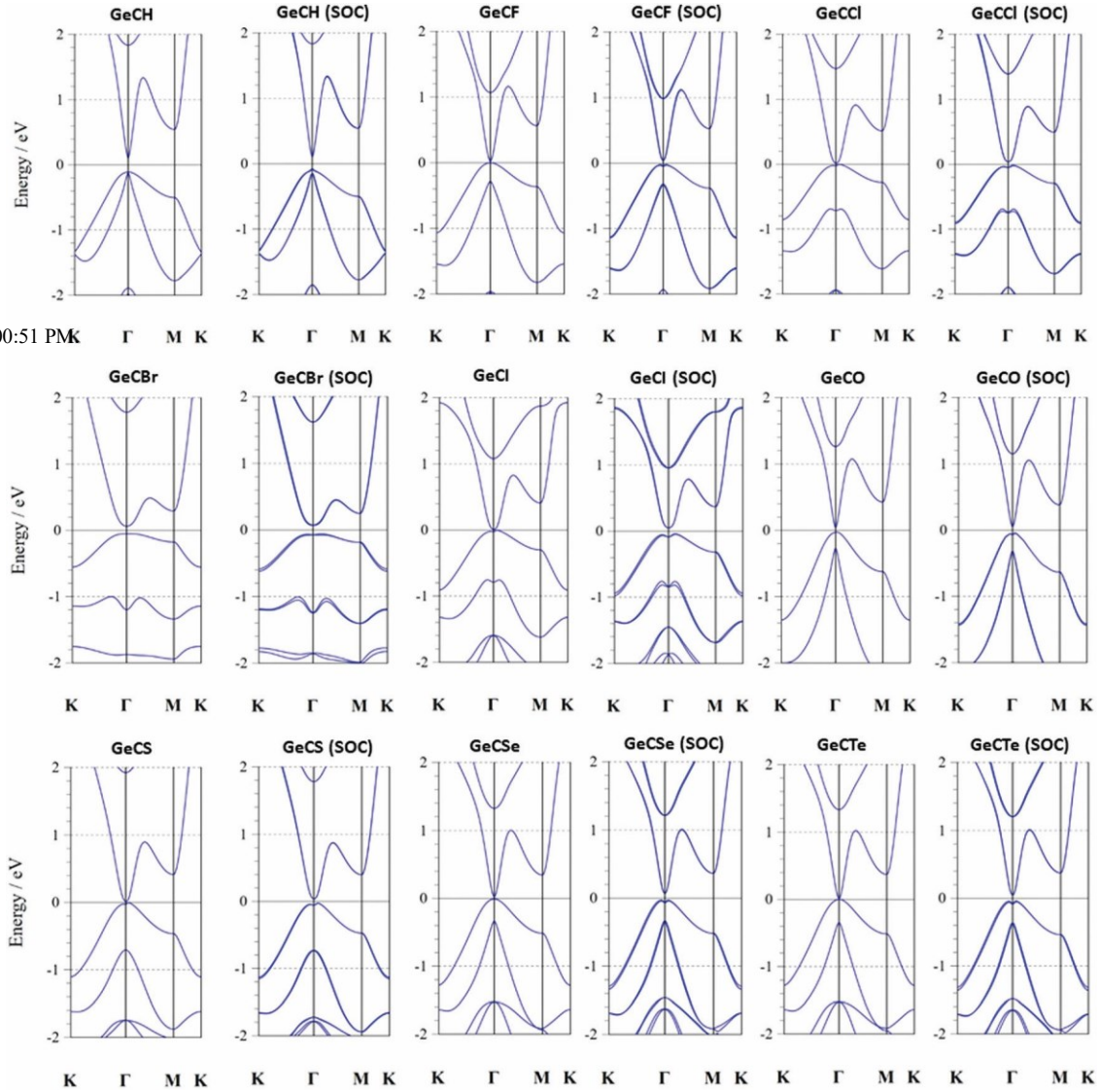

Fig. 6 Calculated band structures of GeCX are shown, both with and without SOC as indicated. The Fermi level is set to 0 eV.

Table 2 List of GeX and GeMX systems exhibiting the QSH effect based on the BHZ model. Green cells are 2D TIs

GeMX System	M=None	M=N	M=P	M=As	M=C
X=H				■	
X=F				■	■
X=Cl			■	■	■
X=Br			■	■	
X=I	■	■	■	■	■
X=O	■		■	■	
X=S				■	■
X=Se	■		■	■	■
X=Te	■	■		■	■

and GeMX systems exhibit a band inversion and enlarged band 0.041 eV to 0.308 eV, all higher than the thermal energy at room gaps after SOC is applied, and thus are TIs exhibiting the QSH temperature of 0.026 eV. Thus, all of these TIs are suitable for effect. The SOC band gaps of the TIs discovered range from room-temperature applications. In addition, our study indicates

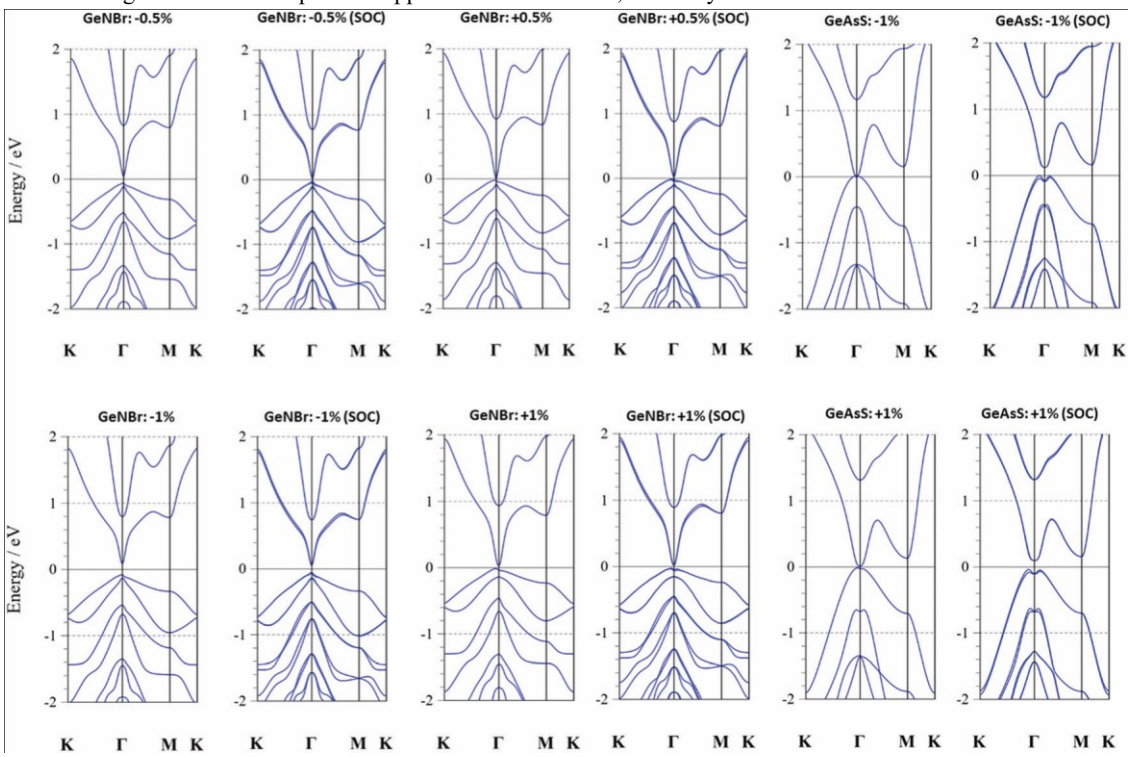

Fig. 7 Effect of intra-layer strain in GeNBr and GeAsS: For GeNBr, the Ge–Ge bond length is tuned by a change of 1%, 0.5%, +0.5% and +1% in comparison with the relaxed structure. There is a remarkable transition from regular insulator to TI at 0.5% strain. The GeNBr is turned back to regular insulator for strain 4 2%, with energy band gap reaching 0.4 eV at 3% strain. From 2% and 2% strain on GeAsS, a 2D TI, the band gap and band inversion are still preserved. GeAsS becomes a regular insulator with strain 4+3%.

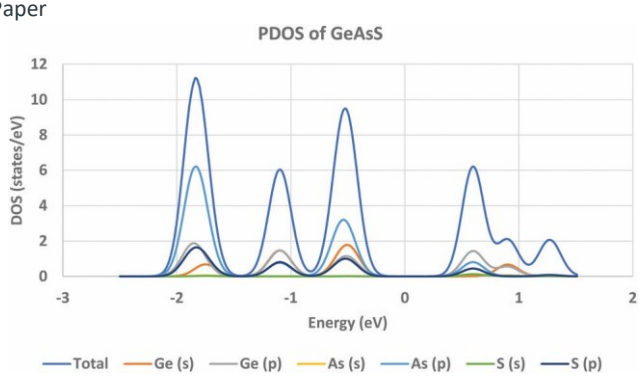

Fig. 8 Calculated partial density of states (PDOS) of GeAsS with SOC. The Fermi level is set to 0 eV.

that regular functionalized germanene insulators can be transformed into 2D TIs via strain engineering.

Such room-temperature applications of TIs include quantum computers, spintronic devices, thermoelectric devices, infrared detectors, exotic particles, image monopoles, and the realization of Majorana Fermions.[10,57–59] TIs also have promising memory cell and magnetic sensor applications.[60] The dissipationless edge transport channels and absence of backscattering of TIs allow for promising applications of these materials in future technology. In the future, we could investigate different M and X atoms, such as transition metals, use other 2D hexagonal structures, or investigate van der Waals heterostructures created by stacking several layers of asymmetrically functionalized germanene together. This study on 2D TIs offers promising options for such room-temperature applications.

Conflicts of interest

There are no conflicts to declare.

Acknowledgements

Q. L. and L. S. acknowledge the support from National Science Foundation grant ECCS-1809399 and Virginia Microelectronics Consortium (VMEC) research seed grant.

References

1 M. Z. Hasan and C. L. Kane, Colloquium: topological insulators, Rev. Mod. Phys., 2010, 82, 3045.
2 X.-L. Qi and S.-C. Zhang, Topological insulators and superconductors, Rev. Mod. Phys., 2011, 83, 1057.
3 B. Yan and S.-C. Zhang, Topological materials, Rep. Prog. Phys., 2012, 75(9), 096501.
4 B. Rasche, et al., Stacked topological insulator built from bismuth-based graphene sheet analogues, Nat. Mater., 2013, 12, 422–425.
5 M. Lang, et al., Competing weak localization and weak antilocalization in ultrathin topological insulators, Nano Lett., 2013, 13, 48–53.
6 J. E. Moore, The birth of topological insulators, Nature, 2010, 464, 194–198.
7 H. Zhang, et al., Topological insulators in Bi_2Se_3, Bi_2Te_3 and Sb_2Te_3 with a single Dirac cone on the surface, Nat. Phys., 2009, 5, 438–442.
8 R.-W. Zhang, et al., Ethynyl-functionalized stanene film: a promising candidate as large-gap quantum spin Hall insulator, New J. Phys., 2015, 17, 083036.
9 L. Kou, et al., Graphene-based topological insulator with an intrinsic bulk band gap above room temperature, Nano Lett., 2013, 13, 6251–6255.
10 L. Wu, et al., New families of large band gap 2D topological insulators in ethynyl-derivative functionalized compounds, Appl. Surf. Sci., 2019, 484, 1208–1213.
11 L. Fu, et al., Topological insulators in three dimensions, Phys. Rev. Lett., 2007, 98, 106803.
12 J. E. Moore and L. Balents, Topological invariants of timereversal-invariant band structures, Phys. Rev. B: Condens. Matter Mater. Phys., 2007, 75, 121306.
13 R. Roy, On the Z_2 classification of quantum spin Hall models, Phys. Rev. B: Condens. Matter Mater. Phys., 2006, 79, 195321.
14 A. Nishide, et al., Direct mapping of the spin-filtered surface bands of a three-dimensional quantum spin Hall insulator, Phys. Rev. B: Condens. Matter Mater. Phys., 2010, 82, 139901.
15 Y. Xia, et al., Observation of a large-gap topologicalinsulator class with a single Dirac cone on the surface, Nat. Phys., 2009, 5, 398–402.
16 B. Andrei Bernevig, et al., Quantum spin Hall effect and topological phase transition in HgTe quantum wells, Science, 2006, 314, 1757–1761.
17 M. Konig, et al., Quantum spin Hall insulator state in HgTe quantum wells, Science, 2007, 318, 766–770. 18 I. Knez, et al., Evidence for helical edge modes in inverted InAs/GaSb quantum wells, Phys. Rev. Lett., 2011, 107, 136603.
19 Y. Ma, et al., Robust two-dimensional topological insulators in methyl-functionalized bismuth, antimony, and lead bilayer films, Nano Lett., 2015, 15, 1083–1089.
20 Y. Xu, et al., Large-gap quantum spin Hall insulators in tin films, Phys. Rev. Lett., 2013, 111, 136804.
21 C. Lee, et al., Measurement of the elastic properties and intrinsic strength of monolayer graphene, Science, 2008, 321, 385–388, DOI: 10.1126/science.1157996.
22 C. Si, et al., Electronic strengthening of graphene by charge doping, Phys. Rev. Lett., 2012, 109, 226802.
23 D. S. L. Abergel, et al., Properties of graphene: a theoretical perspective, Adv. Phys., 2010, 59, 261–482.
24 C. Si, et al., First-principles calculations on the effect of doping and biaxial tensile strain on electron-phonon coupling in graphene, Phys. Rev. Lett., 2013, 111, 196802.

25 H. Min, et al., Intrinsic and Rashba spin-orbit interactions in graphene sheets, Phys. Rev. B: Condens. Matter Mater. Phys., 2006, 74, 165310.

26 C.-C. Liu, et al., Quantum spin Hall effect in silicene and twodimensional germanium, Phys. Rev. Lett., 2011, 107, 076802.

27 C. Si, et al., Functionalized germanene as a prototype of large-gap two-dimensional topological insulators, Phys. Rev. B: Condens. Matter Mater. Phys., 2014, 89, 115429.

28 M. E. Davila, et al., Germanene: a novel two-dimensional germanium allotrope akin to graphene and silicene, New J. Phys., 2014, 16, 095002.

29 L. Kou, et al., Two-dimensional topological insulators: progress and prospects, J. Phys. Chem., 2017, 8, 1905–1919.

30 X. Qian, et al., Quantum spin Hall effect in two-dimensional transition metal dichalcogenides, Science, 2014, 346, 1344–1347.

31 M. A. Py and R. R. Haering, Structural destabilization induced by lithium intercalation in MoS_2 and related compounds, Can. J. Phys., 1983, 61, 76–84.

32 Y. Wang, et al., Atomic mechanism of dynamic electrochemical lithiation processes of MoS_2 nanosheets, J. Am. Chem. Soc., 2014, 136, 6693–6697.

33 Y.-C. Lin, et al., Atomic mechanism of the semiconductingto-metallic phase transition in single-layered MoS_2, Nat. Nanotechnol., 2014, 9, 391–396.

34 J. Li, et al., Topological insulators with tunable band gaps: single-layer HgTe and HgSe, Sci. Rep., 2015, 5, 14115.

35 J. Zhao, et al., Functionalized arsenene (AsX, X = F, OH and CH_3) monolayers with pronounced light absorption, Nanoscale, 2016, 8, 9657–9666.

36 J.-J. Zhou, et al., Quantum spin Hall insulator in single layer bismuth monobromide Bi_4Br, Nano Lett., 2014, 14, 4767–4771.

37 Z. Song, et al., Quantum spin Hall insulators and quantum valley Hall insulators of BiX/SbX (X = H, F, Cl and Br) monolayers with a record bulk band gap, NPG Asia Mater., 2014, 6, e147.

38 M. Pumera and C. H. A. Wong, Graphane and hydrogenated graphene, Chem. Soc. Rev., 2013, 42, 5987–5995.

39 S. Li, et al., Effect of amidogen functionalization on quantum spin Hall effect in Bi/Sb(111) films, ACS Appl. Mater. Interfaces, 2017, 9, 41443–41453.

40 C.-H. Hsu, et al., Quantum anomalous Hall insulator phase in asymmetrically functionalized germanene, Phys. Rev. B: Condens. Matter Mater. Phys., 2017, 96, 16.

41 M. Zhang, et al., Prediction of high-temperature Chern insulator with half-metallic edge states in asymmetryfunctionalized stanene, Nanoscale, 2018, 10, 20226–20233.

42 W. Kohn and L. J. Sham, Self-consistent equations including exchange and correlation effects, Phys. Rev., 1965, 140, A1133.

43 P. Hohenberg and W. Kohn, Inhomogeneous electron gas, Phys. Rev., 1964, 136, B864.

44 P. Giannozzi, et al., Quantum espresso: a modular and open-source software project for quantum simulations of materials, J. Phys.: Condens. Matter, 2009, 21, 395502.

45 G. Liu, et al., Tuning the electronic properties of germanene by molecular adsorption and under an external electric field, J. Mater. Chem. C, 2018, 6, 5937–5948.

46 R. Chegel and S. Behzad, Tunable electronic, optical, and thermal properties of two-dimensional germanene via an external electric field, Sci. Rep., 2020, 10, 704.

47 Z. Ni, et al., The electronic structure of quasi-free-standing germanene on monolayer MX (M = Ga, In; X = S, Se, Te), Phys. Chem. Chem. Phys., 2015, 17, 19039–19044.

48 Z. Yue et al., Topological Insulator Materials for Advanced Optoelectronic Devices, John Wiley & Sons, Ltd, 2019, ch. 2, pp. 45–70.

49 H. Peng, et al., Topological insulator nanostructures for near-infrared transparent flexible electrodes, Nat. Chem., 2012, 4, 281–286.

50 F. Zhang, Topological valleytronics: Brought to light, Nat. Phys., 2018, 14, 111–113.

51 Y. Wang, et al., Density functional theory analysis of structural and electronic properties of orthorhombic perovskite CH3NH3PbI3, Phys. Chem. Chem. Phys., 2014, 16, 1424–1429.

52 I. Aguilera, et al., Spin-orbit coupling in quasiparticle studies of topological insulators, Phys. Rev. B: Condens. Matter Mater. Phys., 2013, 88, 165136.

53 S. Zhang, et al., Semiconductor-topological insulator transition of two-dimensional SbAs induced by biaxial tensile strain, Phys. Rev. B, 2016, 93, 245303.

54 S.-Y. Xu, et al., Topological phase transition and texture inversion in a tunable topological insulator, Science, 2011, 332, 560–564.

55 O. V. Yazyev, et al., Quasiparticle effects in the bulk and surface-state bands of Bi_2Se_3 and Bi_2Te_3 topological insulators, Phys. Rev. B: Condens. Matter Mater. Phys., 2012, 85, 161101(R).

56 L. Kou, et al., Structural and electronic properties of layered arsenic and antimony arsenide, J. Phys. Chem. C, 2015, 119, 6918–6922.

57 J. Schliemann, J. C. Egues and D. Loss, Nonballistic spinfield-effect transistor, Phys. Rev. Lett., 2003, 90, 146801.

58 X.-L. Qi and S.-C. Zhang, Topological insulators and superconductors, Rev. Mod. Phys., 2011, 83, 1057.

59 D. Jariwala, V. K. Sangwan, L. J. Lauhon, T. J. Marks and M. C. Hersam, Emerging device applications for semiconducting two-dimensional transition metal dichalcogenides, ACS Nano, 2014, 8, 1102–1120.

60 T. Fujita, et al., Topological Insulator Cell for Memory and Magnetic Sensor Applications, Appl. Phys. Express, 2011, 4, 094201.